Journal of Applied Informatics and Computing (JAIC)
Vol.10, No.4, August 2026, pp. 3277~3285
e-ISSN: 2548-6861

Mapping Urban Vegetation Change Using RGB-Based K-Means Clustering In Baubau City

Afriningsih Harjunianti [1]*, Syafruddin Syarif [2], Yuyun Wabula [3]***, Abdul Latief Arda [4*], Supriadi Sahibu[5*], Ingrid Nurtanio[6**]**
* Dept. Computer System, Universitas Handayani Makassar
** Dept. Electrical Engineering, Hasanuddin University Makassa
*** Research Center for Data and Information Sciences National Agency for Research and Innovation, BRIN Bandung
afriningsinew@gmail.com[1], ssyariftuh376@gmail.com[2], yuyu010@brin.go.id[3], abdullatief@handayani.ac.id[4],
supriadi@handayani.ac.id[5], ingrid.nurtanio@gmail.com[6]

Article Info

Article history:

Received 2026-05-21
Revised 2026-07-24
Accepted 2026-08-08

Keyword:

K-Means clustering,
Land cover change,
RGB satellite imagery,
Urban ecological monitoring,
Vegetation fragmentation.

ABSTRACT

Urban ecological monitoring is increasingly essential in rapidly developing tropical regions. This study investigates land-cover changes and vegetation dynamics in Baubau City, Indonesia, from 2019 to 2025 using an RGB-based unsupervised classification framework. The primary aim is to develop a practical, cloud-enabled approach for analyzing multitemporal satellite imagery where access to multispectral data is limited. RGB composites were processed using K-Means clustering, Cosine Similarity matrices, and Elbow validation to extract dominant land-cover classes over time. The analysis revealed four major land-cover classes: dense vegetation, mixed vegetation, open land, and built-up areas. A significant ecological disturbance was identified in 2022, characterized by a sudden decline in vegetation and increased spectral similarity across clusters, suggesting both urban expansion and atmospheric interference. By 2023–2025, vegetation began to recover, though in a more fragmented pattern. Sub-clustering of dense vegetation confirmed this shift, with very dense classes giving way to transitional zones. The findings demonstrate the capability of RGB-only methods to produce ecologically meaningful classifications when paired with robust analytical techniques. The study also highlights the benefits of using cloud platforms like Google Earth Engine and Colab for accessible environmental monitoring. These insights support urban planning efforts and encourage the integration of lightweight remote sensing approaches into decision-making processes in resource-constrained settings.

I. INTRODUCTION

Urban vegetation plays a crucial role in supporting ecological functions and environmental quality in rapidly growing tropical coastal cities [2], [12]. It supports climate regulation, heat mitigation, stormwater control, carbon storage, and urban biodiversity. In developing coastal cities, these functions are increasingly critical as rapid population growth and infrastructure expansion intensify environmental pressure. Urban expansion commonly leads not only to vegetation loss but also to fragmentation, edge formation, and spatial reconfiguration of remaining green spaces. These structural changes reduce habitat continuity, weaken ecological connectivity, and erode urban ecosystem resilience. Accordingly, monitoring urban vegetation dynamics requires approaches that capture both overall land-cover change and internal structural transformation.

Monitoring urban vegetation change is therefore essential for sustainable urban planning and environmental management [1], [8]. Long-term observation of vegetation persistence, degradation, and fragmentation supports policy evaluation and risk anticipation in rapidly urbanizing cities. Vegetation change often occurs incrementally through infill development, edge erosion, and gradual encroachment rather than abrupt clearing. Approaches limited to binary land-cover transitions may fail to detect these early structural signals, underscoring the need for monitoring frameworks sensitive to both spatial extent and internal reorganization.

Remote sensing is a primary tool for monitoring land-use and land-cover change at the city scale due to its synoptic coverage, temporal repeatability, and cost efficiency [9], [8]. Multispectral imagery and vegetation indices such as NDVI are widely used to quantify vegetation extent and condition [10], [16]. Supervised machine-learning classifiers further enhance thematic mapping accuracy when reliable reference data are available.

Despite their effectiveness, conventional remote-sensing methods face limitations in rapidly changing or data-limited urban environments. Supervised classifiers depend on consistent, high-quality training data across multiple years [7], which are often unavailable in medium-sized cities. Sensor differences, acquisition geometry, and urban surface heterogeneity further complicate temporal comparison. NDVI-based analyses also assume stable atmospheric conditions and are sensitive to residual noise, making it difficult to distinguish true ecological change from data artefacts in long-term studies.

Data-quality challenges are particularly pronounced in tropical coastal regions. Persistent cloud cover, haze, and illumination variability frequently contaminate optical satellite imagery [3],[4]. Even after cloud and shadow masking, residual artefacts often remain in annual composites [5], [6], potentially generating spurious land-cover transitions. Distinguishing genuine vegetation dynamics from image-quality artefacts thus becomes a central methodological challenge in long-term tropical urban monitoring.

Within this context, the limitations of supervised classification become more evident. Although supervised methods can achieve high accuracy, they require temporally consistent ground reference data that are often unavailable or inconsistent in rapidly developing cities. Unsupervised clustering provides an alternative by reducing dependence on training data and enabling exploratory multi-year analysis [15]. However, its interpretability and stability depend strongly on feature representation and similarity measurement.

Among unsupervised techniques, K-Means clustering remains widely used due to its computational efficiency, conceptual simplicity, and scalability [15], [13]. Conventional implementations rely on Euclidean distance, which is sensitive to brightness variation, haze, and illumination effects. Cosine similarity, by contrast, emphasizes directional relationships between feature vectors and reduces sensitivity to magnitude differences, making it more robust for RGB composites affected by atmospheric variability. This property enhances the temporal stability of clustering results across years [15]. Beyond identifying major land-cover classes, urban vegetation analysis must address internal structural dynamics and fragmentation. Dense vegetation typically degrades gradually into heterogeneous or edge-dominated configurations before large-scale clearing occurs. Sub-clustering within vegetation classes enables examination of increasing heterogeneity and edge dynamics using the same imagery [11], [12], allowing early detection of structural reconfiguration not evident in aggregate statistics. Despite advances in multispectral monitoring and machine-learning-based analysis, few studies integrate annual RGB composites with unsupervised clustering and similarity-based separability diagnostics in cloud-prone tropical cities. In particular, limited work combines cosine-similarity-based K-Means with hierarchical sub-clustering to detect both anomalous observation years and internal vegetation fragmentation. This gap is especially relevant for medium-sized coastal cities, where data limitations necessitate operational and interpretable workflows.

Building on this context, this study examines urban vegetation change in Baubau City, Southeast Sulawesi, Indonesia, using annual true-color (RGB) satellite composites from 2019 to 2025. The workflow applies K-Means clustering with cosine similarity and determines the optimal number of clusters using the elbow method, consistently identifying four interpretable land-cover classes. Cluster separability analysis is used to diagnose anomalous observation years, while sub-clustering within dense vegetation assesses internal fragmentation dynamics. The objective is to develop an operational, reproducible, and uncertainty-aware framework for preliminary detection of urban vegetation change in cloud-prone, data-limited tropical environments.

II. Method

A. Research Flow

Illustrates the overall workflow of the proposed study for multitemporal land-cover analysis in Baubau City using satellite imagery. The workflow consists of image preprocessing, spectral feature extraction (RGB, NIR, and SWIR bands), feature normalization, and unsupervised K-Means clustering. Cluster diagnostics and the Elbow method are applied to determine the optimal number of clusters, while clustering results are further converted from pixel counts into land-cover area estimates to identify vegetation, open land, and built-up areas.

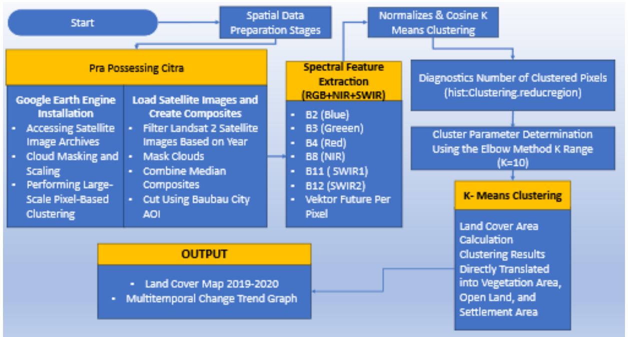

Figure 1. Data flow diagram of method used.

B. *Study Area*

This research focuses on Baubau City, a medium-sized tropical coastal city in Southeast Sulawesi, Indonesia. Baubau's urban form is characterized by a dense built-up coastal core and expanding peri-urban development toward inland vegetated areas. The city is a relevant setting for monitoring urban vegetation change because coastal reclamation, infrastructure growth, and population pressure can accelerate vegetation conversion and fragmentation along urban edges. The analysis extent followed the official administrative boundary of Baubau City to ensure spatial consistency across years.

C. *Data Sources and Temporal Scope*

The study employed annual true-color (RGB) satellite image composites for the period 2019–2025. RGB imagery was selected to maximize accessibility and interpretability in data-limited settings and to demonstrate the feasibility of monitoring when multispectral bands or index products are not consistently available. For each year, all available cloud-screened optical observations within the calendar year were aggregated into one representative composite, enabling interannual comparison while reducing short-term noise. This design supports the study objective stated in the abstract: detecting multi-year vegetation dynamics and identifying anomalous transition periods under cloud-prone conditions

D. *Cloud-Based Preprocessing and Composite Generation*

All image preparation steps were executed in Google Earth Engine (GEE) to ensure reproducibility, scalability, and consistent parameterization across years. Preprocessing consisted of: (i) applying platform-provided cloud and cloud-shadow masking based on quality assessment information, (ii) mosaicking and annual compositing to obtain a single RGB image per year, and (iii) clipping each annual composite to the Baubau City boundary. Because tropical scenes often retain thin clouds, haze, and illumination variability even after masking, residual atmospheric artefacts were treated as a known uncertainty source rather than being assumed fully removed. This assumption is consistent with recent remote-sensing literature emphasizing the persistence of cloud/shadow challenges and the need for methods that can flag low-confidence observations instead of over-interpreting them [10], [11].

E. *Feature Representation and Data Preparation*

Each annual RGB composite was converted into a pixel-level dataset, where each pixel was represented by a three-dimensional feature vector x = [R, G, B]. No vegetation indices or ancillary predictors were used, in order to isolate the information content of RGB and keep the workflow transparent for non-specialist stakeholders. Annual pixel feature sets were exported from GEE and processed in a Python environment (e.g., Google Colab) for clustering, centroid analysis, similarity diagnostics, and visualization. To improve reproducibility, identical preprocessing logic and clustering settings were applied to every year, and random initialization was controlled through a fixed seed.

F. *Unsupervised Land-Cover Clustering*

Land-cover mapping was conducted using K-Means clustering applied independently to each year's RGB pixel vectors. K-Means was chosen because it does not require labeled training data and can provide an operational baseline classification in settings where ground reference data are limited or inconsistent over time. This choice aligns with recent findings that unsupervised clustering can serve as a practical exploratory mapping approach and complement supervised classification when training data constraints are binding [6], [13].

G. *Determining the Number of Clusters*

The optimal number of clusters (K) was selected using the elbow method, computed by evaluating the Within-Cluster Sum of Squares (WCSS) over $K \in \{2,\ldots,10\}$ for each year. The inflection point where additional clusters yielded diminishing reductions in WCSS was taken as the optimal K. Across 2019–2025, the elbow consistently indicated K = 4, supporting statistical stability and thematic interpretability of major urban land-cover groupings.

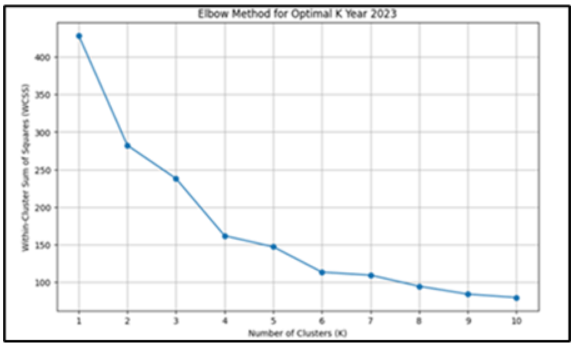

Figure 2 . Elbow-method curves (WCSS vs. K) for annual RGB clustering (2019–2025), showing a consistent inflection point at K = 4.

H. *Similarity-Based Diagnostics Using Cosine Similarity*

While K-Means commonly relies on Euclidean distance for assignment, this study incorporated cosine similarity as a diagnostic tool to evaluate spectral separability between cluster centroids. Cosine similarity emphasizes angular similarity between vectors and is less sensitive to brightness magnitude differences caused by haze or illumination shifts. For each year, cluster centroid vectors c_k = [R_k, G_k, B_k] were calculated, and pairwise cosine similarity values between centroids were computed and visualized as heatmaps. Higher inter-centroid similarity was interpreted as reduced separability and thus greater classification uncertainty for that year, rather than direct evidence of ecological change. This diagnostic is especially relevant in cloud-prone tropical environments where annual composites can differ in visibility conditions [11], [13].

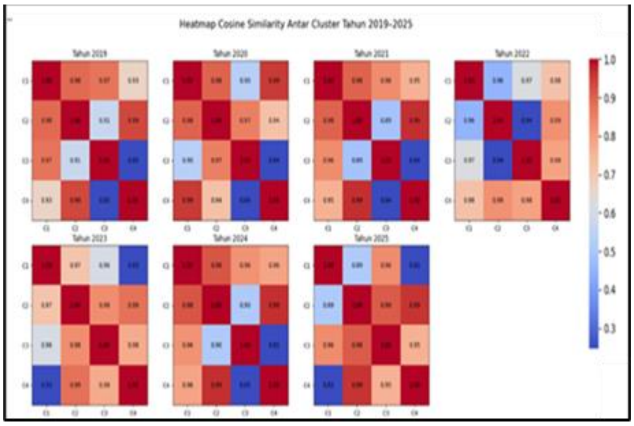

Figure 3. Cosine-similarity heatmaps between K-Means cluster centroids for each year (2019–2025).

I. Cluster Interpretation and Thematic Labeling

The four clusters were interpreted into land-cover groups using a consistent rule set combining: (i) centroid RGB channel dominance and magnitude, (ii) spatial distribution patterns, and (iii) visual comparison with the underlying annual RGB composites. Clusters with relatively high green-channel dominance and contiguous inland patterns were labeled Dense Vegetation, while clusters with moderately elevated green values were labeled Moderate Vegetation. Clusters with low green contribution and concentration in the urban core/coastal corridor were labeled Dense Built-up Areas. Remaining clusters with mixed spectral signatures were labeled Open Land. These labels are intended as interpretable thematic proxies rather than field-validated categories.

TABEL 2. PIXEL-BASED STATISTICS OF LAND-COVER CLASSES IN BAUBAU CITY (2019–2025).

Year	Cluster	Mean					
		B2	**B3**	**B4**	**B8 (NIR)**	**B11 (SWIR1)**	**B12 (SWIR)**
2019	C1	0.13922	0.19632	0.10444	0.04978	0.50441	0.35768
2019	C2	0.09987	0.16256	0.11470	0.07839	0.50879	0.25554
2019	C3	0.22301	0.26946	0.29735	0.15064	0.50361	0.43582
2019	C4	0.20883	0.14236	0.08056	0.07431	0.40691	0.11858
2020	C1	0.06892	0.16078	0.10145	0.08636	0.49003	0.24726
2020	C2	0.14209	0.20609	0.18475	0.67398	0.56306	0.34574
2020	C3	0.23278	0.27311	0.29763	0.51150	0.56074	0.44088
2020	C4	0.08624	0.13998	0.07409	0.87963	0.39899	0.17854
2021	C1	0.14137	0.20043	0.17762	0.60913	0.54736	0.32338
2021	C2	0.09066	0.15510	0.08499	0.82447	0.47425	0.22922
2021	C3	0.23466	0.27381	0.29458	0.52121	0.55514	0.42972
2021	C4	0.08152	0.13412	0.06910	0.88511	0.39450	0.17207
2022	C1	0.29785	0.31394	0.30264	0.59430	0.47341	0.36617
2022	C2	0.22701	0.25112	0.19996	0.79422	0.39222	0.23617
2022	C3	0.40237	0.39035	0.35992	0.61980	0.31088	0.26394
2022	C4	0.31408	0.32160	0.28148	0.72148	0.35477	0.26095
2023	C1	0.24376	0.27355	0.29621	0.56714	0.52264	0.41759
2023	C2	0.19056	0.22702	0.20574	0.73760	0.46897	0.31747
2023	C3	0.29253	0.30625	0.26961	0.72832	0.37631	0.26038
2023	C4	0.13169	0.21202	0.16498	0.26572	0.39916	0.22096
2024	C1	0.16597	0.21792	0.20023	0.70904	0.51323	0.32460
2024	C2	0.11555	0.16737	0.11527	0.81382	0.46855	0.24335
2024	C3	0.24847	0.27737	0.30612	0.51877	0.54441	0.43372
2024	C4	0.09941	0.14536	0.08368	0.87523	0.40153	0.17993
2025	C1	0.23109	0.26971	0.29384	0.49736	0.57070	0.45021
2025	C2	0.09735	0.15475	0.09822	0.81087	0.49014	0.23771
2025	C3	0.14107	0.19947	0.17855	0.68602	0.56095	0.33479

J. Hierarchical Sub-Clustering of Dense Vegetation

To assess internal vegetation structure and fragmentation, a second-stage K-Means clustering was applied only to pixels assigned to the Dense Vegetation class. Dense-vegetation pixels were partitioned into four sub-classes representing very dense, dense, moderate, and mixed/transitional vegetation, based on centroid characteristics and spatial coherence. This hierarchical step targets edge-driven heterogeneity and vegetation thinning patterns that may not be evident in coarse land-cover classes, consistent with recent calls to examine structural transitions rather than net change alone [2].

K. Consistency Checks and Uncertainty-Aware Interpretation

Because the workflow is unsupervised and field ground truth was not available, evaluation emphasized internal consistency and temporal plausibility. Three complementary checks were used: (i) centroid stability tracking across years, (ii) cosine-similarity ranges as a separability indicator, and (iii) cross-year agreement measures (e.g., normalized mutual information and Kappa) between annual classified maps to assess whether transitions were coherent. Years exhibiting unusually high inter-centroid similarity and atypical agreement patterns were flagged as potentially affected by atmospheric/illumination artefacts and interpreted cautiously. This uncertainty-aware design supports the study's aim—outlined in the abstract—to detect both vegetation change and anomalous observation years in data-limited, cloud-prone environments.

III. RESULTS AND DISCUSSION

A. Clustering Structure and Thematic Class Interpretation

This chapter reports the empirical outcomes of the multitemporal RGB-based analysis conducted for Baubau City during 2019–2025 and interprets them in relation to urban ecological monitoring under cloud-prone tropical conditions. Following the workflow described in the methodology, each annual RGB composite was clustered independently using K-Means, and the number of clusters was selected using the elbow criterion. Across all years, the elbow point consistently supported K = 4, indicating that the city's RGB spectral space can be parsimoniously represented by four dominant groupings that remain stable enough to enable temporal comparison. Cross-year stability in cluster structure is important because it reduces the likelihood that year-to-year differences are artefacts of an unstable partitioning scheme rather than changes in land cover. Similar studies of spatio-temporal land use/land cover change detection emphasize that interpretable classes and consistent clustering settings are prerequisites for meaningful temporal inference [13], [17]. The four clusters were interpreted through centroid inspection (relative dominance and magnitude of the R, G, and B channels) and spatial correspondence with recognizable urban morphology. This interpretive step produced four thematic proxies: dense vegetation, moderate vegetation, open land, and dense built-up areas. Because the classification is unsupervised and does not incorporate field-validated labels, the classes are treated as consistent, city-scale thematic groups rather than definitive land-cover categories. Nevertheless, the interpretability of these clusters supports their use for screening interannual transitions and diagnosing potential disturbance years in long-term monitoring, particularly where training data are scarce and repeated ground validation is difficult [5], [13].

(a) year 2019

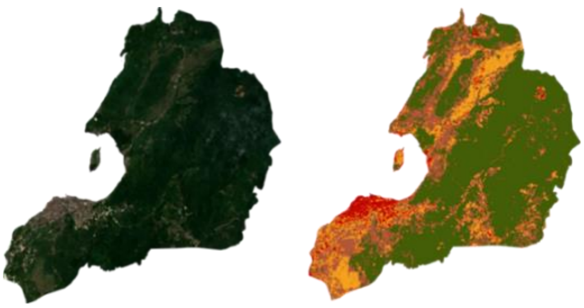

(b) year 2020

(c) year 2021

Figure 4. Land Cover Fluctuations in 2019-2021

B. The 2022 Disturbance: Land-Cover Change or Spectral Anomaly

The pronounced decline in dense vegetation and the concurrent increase in open land and dense built-up classes observed in 2022 represent the most striking feature of the multitemporal analysis. From a land-use perspective, this pattern is consistent with intensified development pressure commonly observed in coastal cities undergoing infrastructure expansion and land reclamation [18]. However, the magnitude of the change exceeds what would typically be expected from land-use transformation alone within a single year.

As discussed in the Results section, the 2022 imagery was affected by higher cloud coverage, and residual cloud and cloud-shadow pixels likely contributed to the misclassification of vegetated areas as non-vegetation classes. This phenomenon has been widely documented in tropical remote sensing studies, where even advanced cloud-masking algorithms cannot fully eliminate atmospheric artifacts [16], [20]. The discussion of 2022 therefore highlights a critical methodological consideration: multitemporal land-cover analysis in cloud-prone regions must be interpreted with caution, and anomalous years should be contextualized using both quantitative indicators and qualitative assessment of data quality. The ability of the proposed system to identify 2022 as an anomalous year rather than a definitive trend underscores its analytical robustness.

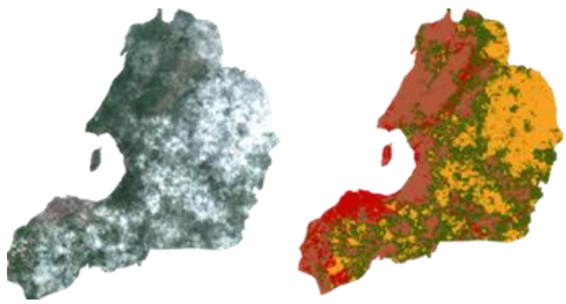

(d) Year 2022

Figure 5. Land Cover in 2022 (Cloud Disturbace Phase)

C. *Vegetation Recovery and the Emergence of a New Equilibrium (2023–2025)*

Following the disturbance observed in 2022, the period from 2023 to 2025 exhibits a clear recovery of dense vegetation and a reduction in open land. This recovery suggests that part of the apparent vegetation loss in 2022 was temporary or artificial, resulting from spectral interference rather than permanent land-cover conversion. At the same time, the sustained increase in moderate vegetation may indicate secondary growth, revegetation of previously open areas, or improvements in image quality that enhance vegetation detectability.

The concept of a "new equilibrium" emerges from the observation that, although vegetation levels recover, dense built-up areas remain higher than during the baseline period. This pattern is consistent with urban land-change theories that describe urbanization as a process in which built-up expansion and vegetation recovery can coexist, particularly when green spaces are preserved or restored as part of urban planning initiatives [3], [10]. The ability of the clustering results to capture this nuanced balance demonstrates the value of multitemporal analysis over single-year assessments.

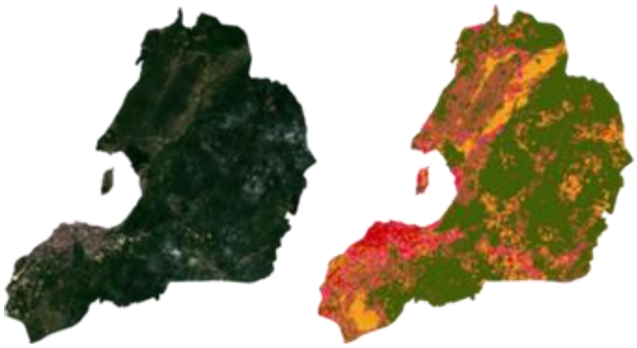

(e) Year 2023

Figure 6 . Land Closure in 2023 (Recovery Phase)

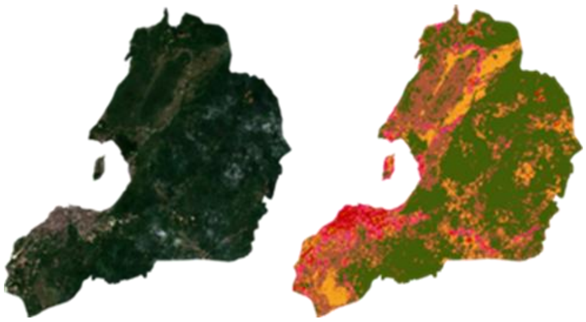

f) Year 2024

g) Year 2025

Figure 7 . Land Cover 2024-2025 (New Stability Phase)

D. *Spatial Patterns of Land-Cover Groups*

The mapped outputs reveal a coherent coastal-to-inland gradient in land-cover proxies that aligns with Baubau's coastal urbanization pattern. Dense built-up areas are concentrated in the urban core and along the coastline, consistent with infrastructural concentration in coastal cities. Dense vegetation appears predominantly inland and in peri-urban zones, where contiguous vegetated patches are retained. Moderate vegetation forms belts and fragments around dense vegetation and at the urban fringe, functioning as transitional zones between more intact vegetation and developed or exposed surfaces. Open land is spatially heterogeneous, appearing in areas of exposed ground, construction, reclaimed/coastal surfaces, and other non-vegetated, non-compact built surfaces.

From a monitoring perspective, these spatial configurations matter because urban ecological degradation in tropical coastal settings often proceeds through edge expansion and fragmentation rather than uniform conversion. Empirical evidence from coastal cities shows that green-space change frequently takes the form of patch contraction and discontinuity, with implications for ecosystem services and well-being [2]. Therefore, stable spatial correspondence between clusters and recognizable land patterns strengthens confidence that subsequent temporal metrics are ecologically interpretable rather than purely statistical artefacts.

E. *Interannual Class Dynamics and Pixel-Based Statistics*

Temporal summaries of class size were derived by counting pixels assigned to each cluster per year (Table 1). During 2019–2021, dense vegetation remained the dominant class, with totals consistently around 1.75 million pixels, indicating a relatively stable baseline. Moderate vegetation and open land remained comparatively stable in this period, while dense built-up areas were the smallest class. Taken together, these baseline years suggest that, at the city-wide scale, the dominant land-cover structure did not undergo abrupt reorganization prior to 2022.

In 2022, the classification shows a pronounced deviation: dense vegetation pixels fall sharply below 1.0 million, while open land and moderate vegetation increase substantially. At face value, such a pattern could be consistent with rapid vegetation clearing or exposure of bare surfaces associated with construction, reclamation, or disturbance. However, 2022 is also the year identified by the study narrative as being strongly affected by extensive cloud cover that reduced surface visibility. In tropical environments, cloud and haze contamination can alter apparent reflectance, obscure vegetation texture, and introduce misclassification when residual artefacts remain in annual composites [9], [10]. For this reason, Table 1 is interpreted jointly with separability diagnostics (Section 3.4) rather than as standalone evidence of ecological conversion.

From 2023 to 2025, dense vegetation partially rebounds relative to 2022, reaching approximately 1.58 million pixels in 2024 and stabilizing around 1.50 million pixels in 2025. Moderate vegetation increases after 2022 and remains elevated by 2025, which is consistent with a structural shift toward more transitional or edge-affected vegetation rather than a full return to pre-2022 conditions. This pattern is consistent with findings from other urban green-space studies indicating that post-disturbance “recovery” can coincide with internal reconfiguration and increased heterogeneity, rather than restoration of intact, contiguous vegetation (Duku et al., 2023).

TABLE I. PIXEL-BASED STATISTICS OF LAND-COVER CLASSES IN BAUBAU CITY (2019–2025).

Cluster	2019	2020	2021	2022	2023	2024	2025
Green (Dense Vegetation)	1,754,901	1,760,213	1,754,801	996,357	1,181,703	1,578,720	1,504,061
Brown (Moderate Vegetation)	724,296	681,667	724,266	885,556	796,897	813,331	929,438
Yellow (Open Land)	339,483	377,952	339,483	813,902	684,728	414,239	371,221
Bright Red (Dense Built-up Areas)	140,564	139,411	140,564	26,349	295,917	152,956	154,526

F. *Cosine Similarity as a Separability and Uncertainty Diagnostic*

Cosine Similarity analysis was employed as a diagnostic tool to evaluate spectral separability among clusters. Pairwise cosine similarity values between cluster centroids ranged from approximately 0.83 to 0.99 across the study period. Lower similarity values indicate greater spectral distinction, while higher values suggest increased overlap and therefore lower separability between classes.

During the baseline years (2019–2021), similarity matrices exhibited heterogeneous patterns, indicating adequate separability among land-cover classes. In contrast, 2022 displayed uniformly high similarity values across most cluster pairs, reflecting reduced spectral differentiation. This reduced separability is consistent with increased atmospheric interference and/or illumination artefacts affecting the 2022 composite, and it supports interpreting 2022 as a year with heightened classification uncertainty. Similarity patterns improved again during 2023–2025, indicating restored separability and improved reliability of the RGB clustering outputs in later years.

G. *Dense Vegetation Sub-Clustering and Fragmentation Signals*

To move beyond coarse thematic classes, the analysis applied a second-stage K-Means clustering to pixels initially classified as dense vegetation. The aim was to characterize internal structural variability within the vegetation mask using four sub-classes (very dense, dense, moderate, and mixed/transitional vegetation) defined by relative RGB centroid characteristics and spatial coherence. This hierarchical strategy is consistent with the broader methodological literature that treats within-class heterogeneity as an informative signal of ecological reconfiguration, particularly where finer multispectral indices are not used or where interpretability is prioritized [18], [19].

The sub-clustering results indicate that 2019–2021 were dominated by very dense vegetation, implying relatively homogeneous vegetative cover within the dense-vegetation mask. In 2022, all vegetation sub-classes decline, aligning with the broader evidence that the year is affected by poor observation quality. Because 2022 is also characterized by reduced centroid separability (Section 3.4), sub-class changes in 2022 are interpreted as uncertain and are not treated as definitive evidence of widespread ecological loss.

From 2023 onward, the composition of the dense-vegetation mask shifts: moderate and mixed/transitional sub-classes increase in relative prominence, and by 2025 mixed/transitional vegetation becomes dominant. This pattern is consistent with a fragmentation or edge-expansion narrative: even if total vegetation area partially rebounds, the internal structure becomes more heterogeneous, suggesting that vegetation patches are increasingly influenced by adjacent development, disturbance, or land-use mixing. Observations from coastal urban green-space studies similarly highlight that fragmentation and the growth of transitional zones can occur alongside partial greening, shaping the functional quality of urban vegetation [2].

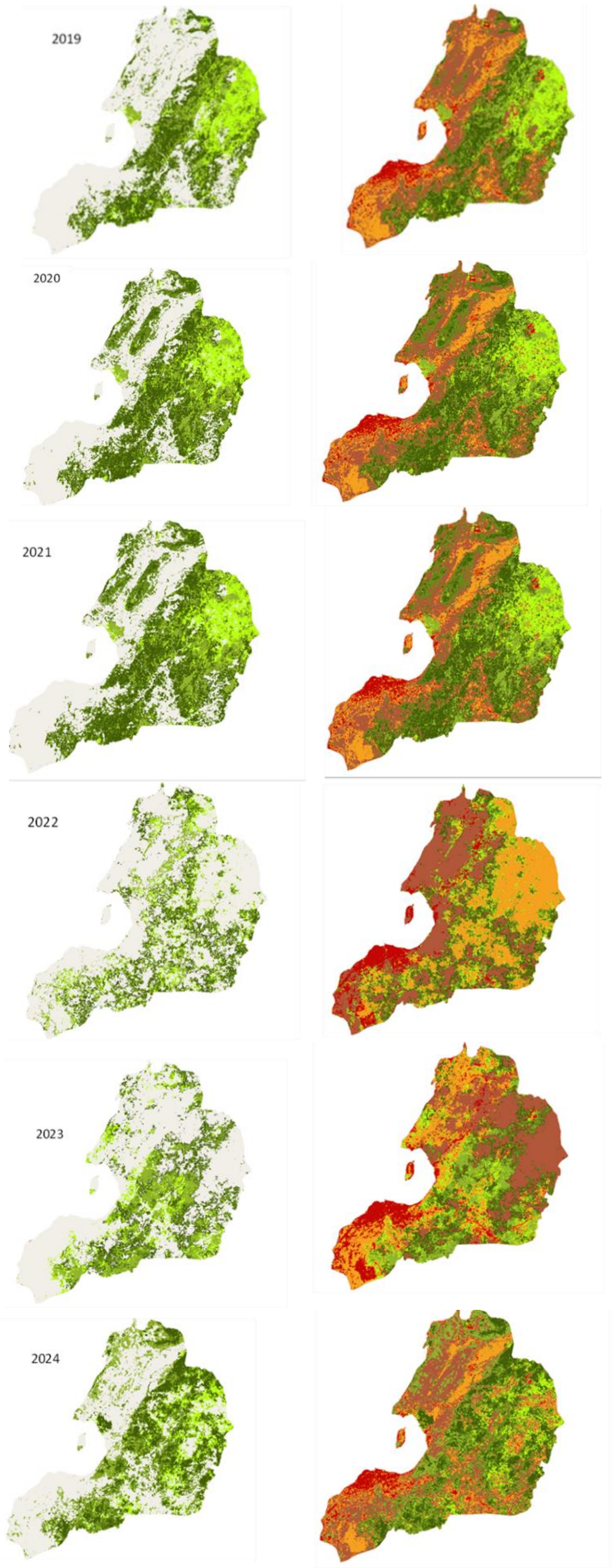

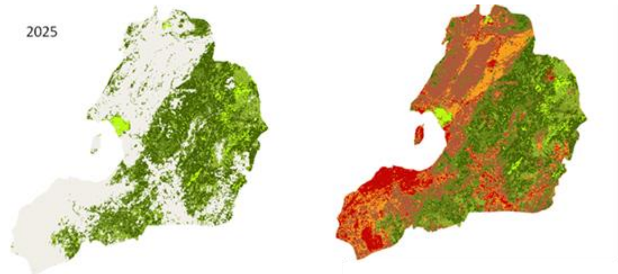

Figure 8. Visualization of dense vegetation sub-clusters and their spatial distribution across selected years.

H. Integrated Interpretation and Implications for Urban Ecological Monitoring

Taken together, the results support a three-phase interpretation of Baubau's land-cover dynamics: (i) a baseline phase (2019–2021) characterized by stable clustering structure, adequate separability, and dominance of dense vegetation; (ii) an anomalous/disturbance phase (2022) marked by abrupt vegetation decline and reduced centroid separability, consistent with substantial cloud contamination and heightened uncertainty; and (iii) a recovery/reconfiguration phase (2023–2025) in which vegetation partially rebounds but exhibits internal heterogenization and increased transitional structure.

Class-area trajectories alone are insufficient for interpreting land-cover change; combining class statistics and centroid-separability diagnostics is necessary [9], [10]. In practical terms, the workflow demonstrates that RGB-only data—when paired with simple but explicit reliability diagnostics—can be used as a screening tool for multi-year urban vegetation monitoring in data-limited environments, complementing more data-intensive multispectral approaches that may not be operationally feasible for local stakeholders.

The study's findings, based on an unsupervised approach, should be interpreted as an uncertainty-aware characterization of urban land-cover patterns. Future work should incorporate targeted ground checks and improved data handling to strengthen inference.

IV CONCLUSION

This study demonstrates that multitemporal urban vegetation and land-cover dynamics in Baubau City (2019–2025) can be meaningfully monitored using an RGB-only, unsupervised framework that integrates K-Means clustering, Elbow-based cluster selection, centroid tracking, and cosine-similarity separability diagnostics on cloud platforms. The results indicate a temporal sequence consisting of (i) a baseline phase of relative vegetation stability from 2019 to 2021, (ii) an anomalous/disturbance phase in 2022 characterized by an abrupt decline in dense vegetation and increases in open land and built-up classes, and (iii) a recovery and reconfiguration phase from 2023 to 2025 in which vegetation partially rebounds while becoming more structurally heterogeneous. Centroid behavior and similarity heatmaps indicate that the 2022 shift is associated with reduced spectral separability and elevated uncertainty, implying that the observed change likely reflects a combination of land transformation signals and residual atmospheric/illumination artefacts, and therefore should not be interpreted as conversion magnitude alone. Dense-vegetation sub-clustering further shows a transition from very dense vegetation dominance toward mixed/transitional vegetation by 2025, consistent with increasing fragmentation nd expanding edge-zone dynamics near urban boundaries. Methodologically, the study contributes a reproducible and accessible pipeline that extends the practical utility of RGB imagery for environmental monitoring where multispectral data, field labels, or advanced infrastructure are constrained, while providing a multi-year vegetation and built-up trajectory for a reclamation-influenced Indonesian coastal city. Future work should incorporate targeted ground validation, stronger cloud and shadow handling, and hybrid RGB–multispectral designs to improve thematic accuracy and enable more reliable forecasting of vegetation and built-up change under alternative planning scenarios.

REFERENCES

[1] A. Dargains and P. Cabral, "A GIS-based Methodology for Sustainable Farming Planning: Assessment of Land Use/Cover Changes and Carbon Dynamics at Farm Level," *Land Use Policy*, vol. 111, p. 105788, 2021, doi: 10.1016/j.landusepol.2021.105788.

[2] E. Duku, C. A. Mensah, I. Amadu, and W. K. Adzigbli, "Changes in Urban Green Spaces in Coastal Cities and Human Well-being: The Case of Cape Coast Metropolis, Ghana," *Geo Geography and Environment*, vol. 10, no. 1, 2023, doi: 10.1002/geo2.119.

[3] F. K. Ahmad, S. S. Kamaruddin, A. H. Ali, and F. L. Ibrahim, "A Feature-Based Optimization Approach for Fake News Detection on Social Media Using K-Means Clustering," in *Commun. Comput. Info. Sci.*, Zakaria N.H., Mansor N.S., Husni H., and Mohammed F., Eds., Springer Science and Business Media Deutschland GmbH, 2024, pp. 125–136. doi: 10.1007/978-981-99-9589-9_10.

[4] S. K. Aryal, H. Prioleau, and G. Washington, "Sentiment Classification of Code-Switched Text Using Pre-Trained Multilingual Embeddings and Segmentation," 2022, doi: 10.5121/csit.2022.122013.

[5] T. Adugna, W. Xu, and J. Fan, "Comparison of Random Forest and Support Vector Machine Classifiers for Regional Land Cover Mapping Using Coarse Resolution FY-3C Images," *Remote Sensing*, vol. 14, no. 3, p. 574, 2022, doi: 10.3390/rs14030574.

[6] R. Ahmed, Md. A. Zafor, and K. Trachte, "Land-Use and Land-Cover Changes in Cottbus City and Spree-Neisse District, Germany, in the Last Two Decades: A Study Using Remote Sensing Data and Google Earth Engine," *Remote Sensing*, vol. 16, no. 15, p. 2773, 2024, doi: 10.3390/rs16152773.

[7] S. Xu, W. Xiao, C. Yu, H. Chen, and Y. Tan, "Mapping Cropland Abandonment in Mountainous Areas in China Using the Google Earth Engine Platform," *Remote Sensing*, vol. 15, no. 4, 2023, doi: 10.3390/rs15041145.

[8] L. S. Galvão, C. Arlanche Petri, and R. Dalagnol, "Coupled effects of solar illumination and phenology on vegetation index determination: an analysis over the Amazonian forests using the SuperDove satellite constellation," *GIScience and Remote Sensing*, vol. 61, no. 1, 2023, doi: 10.1080/15481603.2023.2290354.

[9] D. Moravec, J. Komárek, S. L. Medina, and Í. Molina, "Effect of Atmospheric Corrections on NDVI: Intercomparability of Landsat 8, Sentinel-2, and UAV Sensors," *Remote Sensing*, vol. 13, no. 18, p. 3550, 2021, doi: 10.3390/rs13183550.

[10] Y. Pan, S. Bélanger, and Y. Huot, "Evaluation of Atmospheric Correction Algorithms Over Lakes for High-Resolution Multispectral Imagery: Implications of Adjacency Effect," *Remote Sensing*, vol. 14, no. 13, p. 2979, 2022, doi: 10.3390/rs14132979.

[11] A. Francis, "Sensor Independent Cloud and Shadow Masking With Partial Labels and Multimodal Inputs," *Ieee Transactions on Geoscience and Remote Sensing*, vol. 62, pp. 1–18, 2024, doi: 10.1109/tgrs.2024.3391625.

[12] A. Ahmed, B. Rotich, and K. Czimber, "Assessment of the environmental impacts of conflict-driven Internally Displaced Persons: A sentinel-2 satellite based analysis of land use/ cover changes in the Kas locality, Darfur, Sudan," *PLOS ONE*, vol. 19, no. 5 May, 2024, doi: 10.1371/journal.pone.0304034.

[13] N. Trabelsi, I. Triki, I. Hentati, and N. Rachdi, "Classification and Spatio-Temporal Change Detection of Land Use/Land Cover Using Remote Sensing and Geographic Information System in the Manouba Region, NE Tunisia," *Journal of Geographic Information System*, vol. 15, no. 06, pp. 652–668, 2023, doi: 10.4236/jgis.2023.156033.

[14] D. Dutta, A. Rahman, S. K. Paul, and A. Kundu, "Spatial and temporal trends of urban green spaces: an assessment using hyper-temporal NDVI datasets," *Geocarto International*, vol. 37, no. 25, pp. 7983–8003, 2022, doi: 10.1080/10106049.2021.1989499.

[15] M. A. E. AbdelRahman *et al.*, "Determining the Extent of Soil Degradation Processes Using Trend Analyses at a Regional Multispectral Scale," *Land*, vol. 12, no. 4, 2023, doi: 10.3390/land12040855.

[16] S. Alibakhshi, H. Azadi, and L. Espinosa-Leal, "Can land-use and land-cover change explain reduced resilience in forests?," *Frontiers in Earth Science*, vol. 12, 2024, doi: 10.3389/feart.2024.1317188.

[17] N. I. Utama and D. Pramesti, "Identifying Spatial Patterns of LULC Change with K-Means: A Case Study Using Satellite Data and Google Earth Engine," Institute of Electrical and Electronics Engineers Inc., 2025, pp. 1364–1369. doi: 10.1109/ICoDSA67155.2025.11157344.

[18] M. Trishiani, S. SUGIANTO, T. Arabia, and M. Rusdi, "Vegetation density analysis in Banda Aceh city before and after the tsunami using satellite imagery data," *IOP Conference Series: Earth and Environmental Science*, vol. 951, no. 1. IOP Publishing Ltd, 2022. doi: 10.1088/1755-1315/951/1/012073.

[19] N. I. Utama and D. Pramesti, "Identifying Spatial Patterns of LULC Change with K-Means: A Case Study Using Satellite Data and Google Earth Engine," Institute of Electrical and Electronics Engineers Inc., 2025, pp. 1364–1369. doi: 10.1109/ICoDSA67155.2025.11157344.

[20] N. Gorelick, M. Hancher, M. Dixon, S. Ilyushchenko, D. Thau, and R. Moore, "Google Earth Engine: Planetary-scale geospatial analysis for everyone," *Remote Sens. Environ.*, vol. 202, pp. 18–27, Dec. 2017, doi: 10.1016/j.rse.2017.06.031.